Published in final edited form as:

Nature. 2013 December 12; 504(7479): 291–295. doi:10.1038/nature12748.

High-content genome-wide RNAi screens identify regulators of parkin upstream of mitophagy

Samuel A. Hasson[1,2,*], **Lesley A. Kane**[1,*], **Koji Yamano**[1], **Chiu-Hui Huang**[1], **Danielle A. Sliter**[1], **Eugen Buehler**[2], **Chunxin Wang**[1], **Sabrina M. Heman-Ackah**[3], **Tara Hessa**[1], **Rajarshi Guha**[2], **Scott E. Martin**[2], and **Richard J. Youle**[1]

[1]Surgical Neurology Branch, National Institute of Neurological Disorders and Stroke, National Institutes of Health, Bethesda, Maryland 20892, USA

[2]Division of Preclinical Innovation, National Center for Advancing Translational Sciences, National Institutes of Health, Rockville, Maryland 20850, USA

[3]NIH Center for Regenerative Medicine, Bethesda, Maryland 20892, USA

Abstract

An increasing body of evidence points to mitochondrial dysfunction as a contributor to the molecular pathogenesis of neurodegenerative diseases such as Parkinson's disease[1]. Recent studies of the Parkinson's disease associated genes *PINK1* (ref. 2) and parkin (*PARK2*, ref. 3) indicate that they may act in a quality control pathway preventing the accumulation of dysfunctional mitochondria[4–8]. Here we elucidate regulators that have an impact on parkin translocation to damaged mitochondria with genome-wide small interfering RNA (siRNA) screens coupled to high-content microscopy. Screening yielded gene candidates involved in diverse cellular processes that were subsequently validated in low-throughput assays. This led to characterization of TOMM7 as essential for stabilizing PINK1 on the outer mitochondrial membrane following mitochondrial damage. We also discovered that HSPA1L (HSP70 family member) and BAG4 have mutually opposing roles in the regulation of parkin translocation. The screens revealed that SIAH3, found to localize to mitochondria, inhibits PINK1 accumulation after mitochondrial insult, reducing parkin translocation. Overall, our screens provide a rich resource to understand mitochondrial quality control.

Correspondence and requests for materials should be addressed to R.J.Y. (youler@ninds.nih.gov).
*These authors contributed equally to this work.

Online Content Any additional Methods, Extended Data display items and Source Data are available in the online version of the paper; references unique to these sections appear only in the online paper.

Supplementary Information is available in the online version of the paper.

Author Contributions S.A.H. and R.J.Y. conceived the project; S.A.H., L.A.K., K.Y., D.A.S., C.-H.H., T.H., C.W., S.E.M. and R.J.Y. designed experiments; S.A.H., L.A.K., K.Y., S.M.H.-A., C.-H.H., D.A.S., T.H. and C.W. performed experiments; S.A.H., E.B., R.G. and S.E.M. conducted bioinformatics; and S.A.H. performed the screens. S.A.H., L.A.K. and R.J.Y. wrote the manuscript.

All screening data has been deposited into PubChem under the assay IDs 651811 (non-pooled screen, with siRNA sequences) and 651810 (pooled screen).

The authors declare no competing financial interests.

Readers are welcome to comment on the online version of the paper.

Following the loss of mitochondrial membrane potential, PINK1 and parkin coordinate a ubiquitination[9], proteasomal activation[10] and autophagic (mitophagy)[5] response that may attenuate cell death[11]. As mitophagy can ameliorate the deleterious consequences of mitochondrial dysfunction[12–14], genes regulating parkin translocation could be useful drug targets for increasing mitochondrial quality control. To identify genes important for the PINK1-dependent recruitment of parkin to damaged mitochondria, we conducted genome-wide siRNA screens against two diverse libraries. Our approach used the well-characterized cellular phenotype of parkin accumulation on depolarized mitochondria[5]. HeLa cells stably expressing GFP–parkin (Extended Data Fig. 1a) and a mitochondrial-targeted red fluorescent protein (mito-dsRed) were transfected with siRNA duplexes in 384-well plates (Extended Data Fig. 1b). After siRNA treatment, mitochondria were chemically depolarized with carbonyl cyanide *m*-chlorophenyl hydrazine (CCCP) to induce parkin translocation. Chemical depletion of mitochondrial membrane potential ($\Delta\psi$) mimicked pathological conditions caused by genetic mutation in mitochondrial- or nuclear-encoded genes or other stresses that deplete $\Delta\psi$. The degree of Parkin translocation was then assessed by high-content microscopy and automated image analysis that extracted a multitude of phenotypic parameters (Extended Data Figs 1c, d and 2a, b). *PINK1* siRNA-treated wells served as positive controls, abolishing parkin translocation following CCCP treatment (Fig. 1a). We observed a high degree of assay robustness (Z' >0.5, Extended Data Fig. 2c, d) and technical reproducibility (Extended Data Fig. 2e, f) in primary screens. Assay termination before saturation (Extended Data Fig. 2g) allowed us to detect both translocation inhibitors and accelerators (Extended Data Fig. 2h). For example, *LMAN1* siRNAs accelerated parkin translocation, suggesting the gene negatively regulates this process (Fig. 1a). Our imaging-based assay was used to screen genome-wide arrays of Ambion single (3 unique siRNAs per gene) and Dharmacon pooled (pool of 4 unique siRNAs per gene) reagents to maximize discovery potential.

Candidate gene selection used the robust statistical measure of median absolute deviation (MAD) to standardize siRNA activities from the screens (Fig. 1b, c). Normalized data were analysed using both parkin translocation and cytotoxicity (cell count) measures (see Supplementary Methods and Extended Data Fig. 3). Mito-dsRed intensity was used to identify siRNAs that depleted mitochondria (Extended Data Fig. 3). As important modulators of parkin translocation may have been masked by low-potency gene knockdowns, selection of active reagents at lower thresholds was feasible with our non-pooled siRNA data set, where we observed coincident activity of unique siRNAs with the same gene target. After filtering for cytotoxic or mitochondria depleting siRNAs, a gene was chosen as a ‘candidate’ modulator if at least two siRNAs from the non-pooled data set were active based on phenotypic evaluation of parkin translocation (generally >1.5 MAD or <−1.5 MAD, Extended Data Fig. 4a, b). Pooled siRNA screen candidate selection criteria were set to yield similar numbers of genes as the non-pooled siRNA screen (~±2 MAD, see Supplementary Methods). The candidate list (Supplementary Table 1) had a gene selection rate (see Supplementary Methods) similar to other large-scale RNAi (RNA interference) screens[15]. Twenty-four candidates overlapped between the two screens (Fig. 1c, yellow dots) including an ubiquitin-conjugating enzyme (*UBE2J2*) and a member of the Hedgehog pathway (*HHAT*). Additionally, knockdown of the predicted LOC401052 strongly

accelerated parkin translocation with all four reagents tested. The limited number of shared candidates was consistent with previous studies[16,17].

A large number of initial candidate selections were involved in gene expression (17% of non-pooled, 24% of pooled candidates). As PINK1 is very labile and essential for parkin translocation[6], the high rate of activity from housekeeping gene siRNAs suggests they may influence *PINK1* expression. *PINK1* also may be a source of off-target effects that confound RNAi screens[18–20]. The non-pooled siRNA screening data enabled us to systematically profile the miRNA-like effects of the siRNA seed sequences. Complementarity between the 5′ end or 'seed' region of the siRNA guide strand and the 3′ untranslated region (UTR) of unintended messenger RNAs is a driver of off-target behaviour[20,21]. Seed sequences matching the 3′ UTR of *PINK1* exerted a highly biased inhibitory effect ($P < 2.2 \times 10^{-16}$) on parkin translocation compared to all other siRNA seeds in the library (Extended Data Fig. 4c). We also observed that strongly inhibitory siRNAs (>2 MAD) had ~10% more matches to the 3′ UTR of *PINK1* than the corresponding accelerator siRNAs (Extended Data Fig. 4d). In total, 10,935 siRNAs (~17%) in the non-pooled screen had at least one hexamer[22] seed match to the *PINK1* 3′ UTR. To combat off-target effects we used common seed analysis (CSA)[23]. CSA exposes the activity of siRNA seed-based off-target effects by weighting each reagent against the population of siRNAs in the screen sharing the same seed (Extended Data Fig. 4e–g). The gene-level scoring of the entire non-pooled data set was adjusted for seed bias (Supplementary Table 2). Analysis of C911 mismatch controls[24] supported the hypothesis that siRNAs with strong seed bias (low seed-adjusted *Z*-score) modulate parkin translocation predominantly though seed-driven off-target activity (Extended Data Fig. 4h). In addition to CSA, we used gene pathway enrichment on the original non-pooled screen candidates (Supplementary Table 1) as a complimentary method to identify promising genes. While confirming the strong influence of gene expression modifiers in our non-pooled screen candidates, enrichment analysis (Fig. 2a) revealed the significant ($P < 0.05$) presence of pathways including muscle function, the ubiquitin-proteasome, and autophagy (Supplementary Table 3). Furthermore, queries of the original non-pooled candidates (Supplementary Table 1) against annotated databases (gene ontology (GO) and human MitoCarta) revealed ubiquitin and mitochondrial processes (Supplementary Tables 4 and 5). Within enrichment groups, STRING database analysis (see Supplementary Methods) indicated many putative gene interactions that may regulate parkin (Fig. 2b, c).

To query candidate genes for follow-up, we chose from four distinct categories (Supplementary Table 6). These categories were top performing genes in the seed-adjusted primary screening data (category 1); candidates within a pathway enrichment group (category 2); top candidates from the pooled screen (category 3), and rational selection of candidates guided by gene annotations (category 4). In total, 106 positive regulators of parkin translocation were selected for validation (Supplementary Table 6). Four additional siRNAs from a different vendor were used for high-throughput validation. We found 67 genes in follow-up studies recapitulated parkin translocation inhibition activity with at least two additional siRNA reagents (Fig. 2d), a common reconfirmation benchmark. This cutoff was further substantiated by quantitative PCR with reverse transcription (qRT–PCR) of randomly selected candidates with only 1 active follow-up siRNA (of 4). In all cases,

equivalent knockdown of target mRNA was achieved by both parkin translocation inhibitory and non-active siRNAs in the set (Extended Data Fig. 5a–f). Therefore, on-target knockdown was unlikely to be source of the translocation phenotype in these low confidence reconfirmations. The 67 confirmed candidates were ranked by the number of active siRNA reagents out of the 8 assayed (4 from primary screens and 4 from follow-up analysis) and then by seed-adjusted *Z*-score (Top 10 in Fig. 2e and complete list in Supplementary Table 7). For 8 of the top-ranked genes, we examined mRNA levels in cells transfected with primary screen active siRNAs and observed >75% target knockdown in all but 1 of the 18 siRNAs tested (Extended Data Fig. 5g–n). Secondary screening of active follow-up siRNAs for PINK1 (expressed without its endogenous 3′ UTR) immunofluorescence after CCCP treatment established if these gene knockdowns affected PINK1 protein accumulation (Fig. 2e, red, and Supplementary Tables 7 and 8).

TOMM7, a component of the protein translocase of the outer mitochondrial membrane (TOM) complex, was a reconfirmed candidate from the non-pooled screen and the sixty-third most potent positive regulator of parkin translocation in the seed-adjusted data set. Knockdown of this MitoCarta member in the pooled siRNA screen also showed a translocation deficit. Interestingly, a report on mammalian TOMM7 demonstrated that gene knockdown did not change the efficiency of mitochondrial protein import[25]. Our *TOMM7* gene knockdowns in HeLa cells resulted in a reduction of GFP–parkin translocation ($P < 0.001$, Extended Data Fig. 6a, b) and a reduction of *TOMM7* mRNA levels ($P < 0.001$, Extended Data Fig. 6c). To confirm *TOMM7* siRNA activity was not an off-target effect, we generated a knockout HCT116 cell line using transcription activator-like effector nuclease (TALEN) mediated genome editing (see Supplementary Methods). Wild-type mRNA and protein was undetectable in the *TOMM7* knockout cell line (Extended Data Fig. 6d, e), but *PINK1* mRNA expression was unchanged (Extended Data Fig. 6f). Notably, the knockout of *TOMM7* abolished the translocation of YFP–parkin after CCCP treatment (Fig. 3a, b and Extended Data Fig. 6g). Expression of HA-tagged *TOMM7* in knockout cells restored the YFP–parkin translocation to near wild-type levels ($P < 0.001$ for partial and complete translocation). We examined if *TOMM7* knockout affects mitophagy downstream of parkin translocation. After 24 h exposure to CCCP, <5% of *TOMM7* knockout HCT116 cells underwent detectable mitophagy compared to ~90% of the wild-type cells ($P < 0.001$) (Fig. 3c and Extended Data Fig. 7a). We also observed a deficit in parkin-dependent degradation of MFN1 in knockout cells (Fig. 3d).

To explore TOMM7 function, we evaluated PINK1 levels in *TOMM7* wild-type and knockout HCT116 cell lines. PINK1 undergoes rapid turnover in polarized mitochondria[6] and only trace amounts of PINK1 were detected in cell lysates from both lines (Fig. 3d). However, after CCCP treatment, normal accumulation of full-length PINK1 (ref. 6) failed to occur in *TOMM7* knockout cells, suggesting that TOMM7 is important for PINK1 stabilization on the outer mitochondrial membrane of damaged mitochondria. To explore why, we performed *in vitro* import of radiolabelled PINK1 protein into isolated mitochondria from wild-type or *TOMM7* knockout cells. Mitochondria from both cell lines were similar in their ability to import and process PINK1 precursor protein, as indicated by the amount of PARL-cleaved PINK1 (ref. 26) at each time point (Extended Data Fig. 7b, c). *In vitro* protein import and processing of the canonical Su9–DHFR precursor was also

normal in *TOMM7* knockout mitochondria (Extended Data Fig. 7d, e). When Δψ is depleted, PINK1 associates with the TOM complex in the outer mitochondrial membrane[27]. However, PINK1 imported *in vitro* into TOMM7 knockout mitochondria failed to associate with the TOM complex (Fig. 3e, −Δψ lanes). Our results indicate that human TOMM7 functions in the TOM complex, not for generalized protein import, but to shunt and retain PINK1, and perhaps other proteins, to the surface of damaged mitochondria (Extended Data Fig. 7f).

To explore the wider importance of TOMM7, we depleted *TOMM7* gene expression in human induced pluripotent stem cell (iPS cell) derived neurons (Extended Data Fig. 7g–l). Lentiviral short hairpin RNA (shRNA) achieved a modest knockdown of *TOMM7* mRNA, without affecting *PINK1* mRNA levels (55–75%, Extended Data Fig. 7m, n). As in other cell types, significantly less endogenous PINK1 accumulated following mitochondrial depolarization in *TOMM7* knockdown neurons (Fig. 3f, g, $P < 0.001$ as compared to control). This suggests that TOMM7 functions to recruit parkin to damaged mitochondria by stabilizing PINK1 in neurons expressing tyrosine hydroxylase (TH^+).

In search of positive regulators of parkin function, we were intrigued by *HSPA1L*, a confirmed follow-up selection (category 4, annotation/phenotype-based). As other HSP70 family members can interact with parkin[28,29], HSPA1L may selectively promote parkin translocation activity. HSPA1L is a widely distributed, but low-abundance member of the HSP70 family[30]. The non-pooled siRNA screen yielded *BAG4* as a negative regulator of parkin translocation. BAG-domain-containing proteins act as nucleotide exchange factors for HSP70 members and BAG5 can modulate the E3 ubiquitin ligase activity of parkin[29]. We proposed that HSPA1L and BAG4 co-regulate parkin localization following mitochondrial damage. *HSPA1L* knockdown in HeLa cells led to a significant ($P < 0.01$) decrease in parkin translocation (Extended Data Fig. 8a–c) and *BAG4* knockdown enhanced parkin translocation ($P < 0.001$, Extended Data Fig. 8d–f). Neither of these knockdowns affected the level of PINK1 protein accumulation (Extended Data Fig. 8f, g). To ensure the phenotype was specific to *HSPA1L*, we used TALEN genome editing to knockout *HSPA1L* in HEK293 cells (see Supplementary Methods and Extended Data Fig. 8h). Parkin translocation was strongly inhibited in the *HSPA1L* knockout cells ($P < 0.001$, Fig. 4a, b) that have normal levels of HSPA1A (a homologous, more abundant HSP70), and equivalent levels of PINK1 (Extended Data Fig. 8i, j). This inhibition of parkin translocation was rescued by exogenous mCherry–*HSPA1L* (Fig. 4a, b and Extended Data Fig. 8k). Expression of exogenous *HSPA1A* did not rescue the *HSPA1L* knockout phenotype, indicating the translocation deficit is not from a loss of cytosolic chaperone capacity (Fig. 4b). To investigate the mechanism of HSPA1L modulation of parkin, mutations were introduced into conserved domains: the ATPase domain (Lys73Glu), the Hsp40 binding domain (Leu396Asp), and a truncation in the regulatory/binding region of the carboxyl terminus (ΔEEVD) (see Supplementary Methods). None of these mutants rescued the translocation deficit of the *HSPA1L* knockout cells ($P < 0.01$, Fig. 4b). GFP–parkin immunoprecipitation from the HeLa cell line used in the screens was found to bind endogenous HSPA1L and other HSP70 isoforms by mass spectrometric analysis (Extended Data Fig. 8l and Supplementary Table 9). Immunoprecipitation of HA–BAG4 demonstrates that YFP–parkin also binds to BAG4 and this binding is diminished following mitochondrial

depolarization ($P < 0.01$, Fig. 4c, d). The reciprocal immunoprecipitation of YFP–parkin also shows HA–BAG4 binding to both full-length and to the ΔUBL (ubiquitin-like domain) form of parkin, with stronger binding to the ΔUBL form (Extended Data Fig. 9a). A different BAG domain containing protein, BAG5, had been previously shown to interact with parkin[29]. We confirmed this binding, but observed a greater binding to HA–BAG4 (Extended Data Fig. 9b). RNAi knockdown of *BAG4* or *HSPA1L* alone promotes or inhibits parkin translocation, respectively. However, simultaneous knockdown of both genes in either HeLa (Fig. 4e and Extended Data Fig. 9c) or BE(2)-M17 neuroblastoma cell lines (Extended Data Fig. 9d, e) reduces their respective individual phenotypes. Therefore, neither protein is uniquely required for parkin translocation, but rather an imbalance between them causes robust phenotypes. BAG4 and HSPA1L appear to act together to regulate parkin translocation (Extended Data Fig. 9f).

We assessed the effect of HSPA1L on the translocation of disease-associated parkin mutants[6]. In HeLa cells *HSPA1L* enhanced the translocation of YFP–parkin(R275W) ($P > 0.001$, Fig. 4f, g and Extended Data Fig. 9g) to a greater extent than *HSPA1A*. Future studies on the molecular details of these interactions may provide attractive targets to enhance selective removal of damaged mitochondria.

As the siRNA retesting of negative parkin translocation regulators did not consistently recapitulate the generally more subtle acceleration phenotype, we used the seed-adjusted data set (Supplementary Table 2) to guide the pursuit of these genes. As the tenth most potent seed-adjusted negative regulator, the common seed plot for *SIAH3* siRNAs showed a consistent departure from their seed ‘peers’ (Extended Data Fig. 4g). SIAH3–Myc (SIAH/SINA superfamily member, see Extended Data Fig. 10a) co-localized with mitochondria (Extended Data Fig. 10b, c). We did not detect a stable interaction of SIAH3 and PINK1 in the presence of detergents required for immunoprecipitation (Extended Data Fig. 10d). *SIAH3* knockdown in HeLa cells accelerated parkin translocation with an increase in partially translocated parkin at 30 ($P < 0.001$) and 60 ($P < 0.05$) minutes post CCCP treatment (Extended Data Fig. 10e, f) and complete translocation at 60 min ($P < 0.001$). RNAi rescue by *SIAH3* cDNA expression (siRNA-resistant) significantly ($P < 0.01$) suppressed the complete parkin translocation phenotype (Extended Data Fig. 10e, f). We confirmed the SIAH3-mediated parkin translocation phenotype ($P > 0.01$) and >90% knockdown of *SIAH3* mRNA in BE(2)-M17 neuroblastoma cells stably expressing parkin and mito-GFP ($P > 0.001$, Extended Data Fig. 10g–i). *SIAH3* silencing increased PINK1 accumulation after CCCP treatment ($P > 0.001$, Extended Data Fig. 10j, k). SIAH3 probably acts as a negative regulator of PINK1 stabilization because knockdown of *SIAH3* did not increase *PINK1* mRNA or protein before mitochondrial damage (Extended Data Fig. 10j–l).

In conclusion, we used a diverse siRNA screening strategy to shed light on the genes regulating PINK1-dependent parkin translocation to damaged mitochondria. Using several analysis methods in parallel allowed us to identify and overcome the significant susceptibility of parkin translocation to off-target/pleiotropic *PINK1* modulation and select strong candidates for further study. Our subsequent validation demonstrated unique molecular functions of HSPA1L, BAG4 and SIAH3, as well as defining a role for TOMM7

in outer mitochondrial membrane PINK1 stabilization. Our genome-wide analysis of *PINK1* and parkin regulators illuminates mechanisms of mitochondrial maintenance.

METHODS SUMMARY

siRNA screening

siRNAs were arrayed in 384-well optical plates (2 μl per well, 0.8 pmol). For each well, 20 μl of DMEM medium (Life Technologies) containing 4 μl ml^{-1} RNAiMAX (Life Technologies) was added. After 30 min incubation, 20 μl of a 37,500 cells per ml suspension was added to each well for reverse transfection. Plates with cells were incubated at 37 °C/5% CO_2 for 48 h and the parkin translocation assay was initiated with 40 μl of DMEM containing CCCP (Sigma) at a final concentration of 10 μM. After 2.5 h of incubation with CCCP, cells in all wells were fixed, nuclear stained and analysed using an ImageXpress Micro (Molecular Devices). All screening was performed in environmentally controlled enclosures with automated liquid and plate handling. See Supplementary Methods for detailed methods.

Extended Data

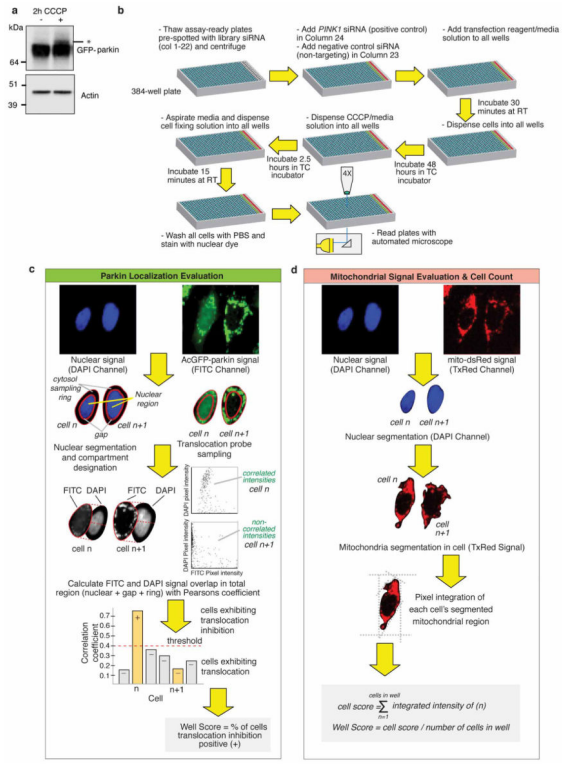

Extended Data Figure 1. Automated screening strategy and image analysis for the parkin translocation assay

a, GFP–parkin expression in the HeLa screening cell line. Ubiquitinated GFP–parkin (*) indicates parkin activation in the presence of CCCP. **b**, The screening workflow used ‘assay-ready’ 384-well plates pre-printed with 0.8pmol of library siRNAs. Non-targeting siRNAs

(green wells) and *PINK1* siRNAs (red wells) were in columns 23 and 24. Cells were reverse transfected with siRNAs 48 h before the parkin translocation assay (addition of 10 μM CCCP). Parallel plate scheduling ensured that the timing of each step in the protocol was consistent across all plates and minimized total length of the screening run. An 8-head peristaltic and 16-head syringe-pump microplate dispensers dispensed reagents during the assay and BioTek EL406 192-tube microplate washer/dispensers were used to remove media and wash. Screening was performing in an environmentally controlled robotic enclosure. High-content microscopy images encompassed the entire cell population of each well. RT, room temperature. All imaged wells were processed with two algorithms from the Molecular Devices MetaXpress PowerCore Server Suite. **c**, Assessment of parkin translocation exploited the loss of GFP–parkin signal in the nuclear region (in the *z*-plane) that occurred as parkin accumulated on mitochondria. Utilization of nuclear-to-cytosol correlation yielded a more robust measure of parkin translocation than measuring GFP–parkin co-localization with mito-dsRed since the latter technique was highly affected by cellular morphology. The automated image analysis algorithm first segmented each cell's nuclear regions by performing top hat and h-dome feature recognition on the Hoechst 33342 staining (DAPI channel image) intensity. Nuclear segmentation created defined 'windows' to observe the level of GFP–parkin. These windows were extended by a 3 pixel gap to correct for imperfect channel overlay. Each cell in the image (n, $n + 1$, and so on) was then interrogated for pixel intensity overlap of the GFP signal (FITC channel image) in the window using a Pearson's correlation that also sampled pixel intensity in a ring (one-third the width of the nuclear window) that extended into the surrounding cytosol (as a signal reference). After calculating the Pearson's correlation of the FITC and DAPI image on the total region comprised of the nuclear window, gap and extended ring, cells scoring over a correlation threshold were scored as positive for parkin translocation inhibition. Well-level translocation data was reported as the percentage of cells in the well over the correlation threshold (exhibiting a lack of parkin translocation). **d**, Cell count and assessment of the mitochondrial signal from the cells in each well was accomplished with the same morphological filters as in **c**. Cell count was determined through the number of segmented nuclei in the DAPI channel image. Using the nuclear segmentation, the algorithm identified the mitochondrial mass associated with each nucleus in the TxRed channel image. The mito-dsRed signal was then integrated across the segmented mitochondrial region for each cell (n, $n + 1$, etc.). Well-level mitochondrial signal was reported as the mean of the cell population's values. See Supplementary Methods for complete details.

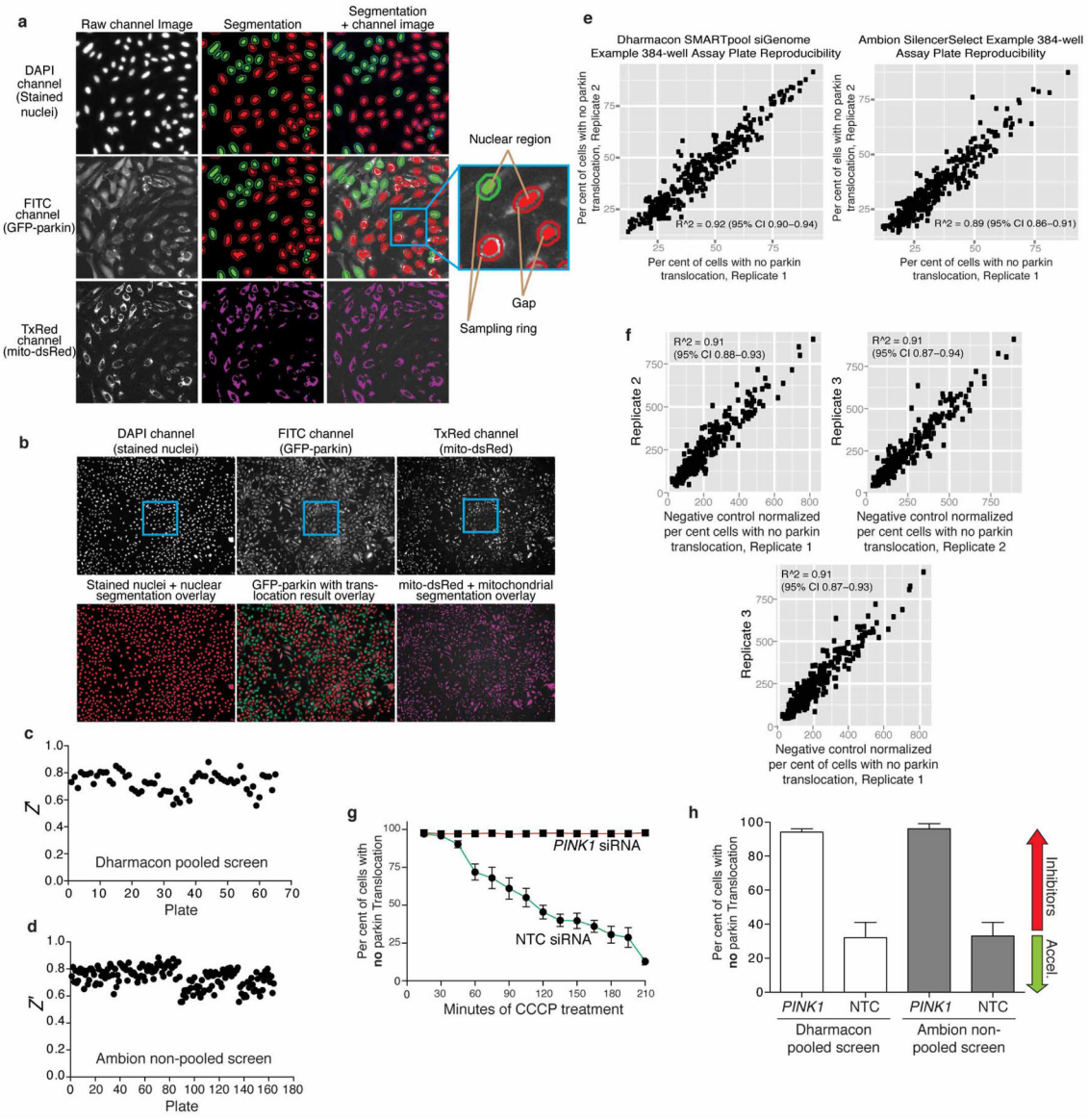

Extended Data Figure 2. Segmentation examples and screen reproducibility

a, Example segmentation of nuclei (solid red or green spots overlaid on DAPI channel images in top panels) along with the scoring of GFP–parkin translocation (FITC channel image). For parkin translocation overlays in middle panels, translocation negative cells are delimited in green; translocation positive cells in red. Segmentation of mitochondrial mass associated with each segmented nuclei is delimited by magenta overlay in bottom panels. **b**, Zoomed-out well images, blue box defines regions in **a**. Translocation overlay is shown for both the DAPI and FITC channels with mitochondrial segmentation shown for the TxRed channel. **c**, The average and standard deviation of the control siRNAs (*PINK1* and NTC) on each plate were used to calculate Z' scores across the Dharmacon pooled siRNA screen. **d**, Same as in **c**, but for the Ambion non-pooled siRNA screen. **e**, Randomly selected library plates from the pooled and non-pooled siRNA libraries were used to make duplicate assay

plates and were run and imaged using the conditions of the original screens. After image analysis and quantification, raw parkin translocation data was plotted from the replicates and correlation was assessed for the non-pooled Ambion (right) and pooled Dharmacon (left) siRNAs. **f**, Additionally, triplicate copies of a Qiagen follow-up 384-well plate containing siRNAs sets for target reconfirmation were run in the automated parkin translocation assay. Translocation scores from each plate were normalized to a percentage of the mean NTC negative control score and plotted relative to one another. These experiments demonstrated a high degree of technical reproducibility for the parkin translocation assay present in both raw and normalized data. **g**, To understand the rate of parkin translocation in the automated assay, a time course format in a similar manner as described for the primary screen was assessed (see Supplementary Methods). Automated plate and liquid handling was performed on the Agilent robotic platform to execute the translocation assay (CCCP dispense, incubation, plate fixing). Successive plates were automatically fixed at intervals of 15 min, nuclear stained and imaged on the high-content microscope (as in the original screens). After automated image analysis, data from 45 wells (per siRNA treatment) per plate were plotted as mean ± s.d. from each time point. Data points from *PINK1* siRNA wells (squares) and data points from NTC siRNA wells (circles) are plotted. Parkin translocation rates presented are specific to large-scale automated screening in 384-well plates. Owing to differences in cell types, culture environment, temperatures and liquid handling factors, parkin translocation rates differed in low-throughput experiments and were therefore calibrated on an experiment-specific basis. **h**, The mean ± s.d. of control reagents from each screen was plotted to illustrate the signal window for parkin translocation assessment (pooled screen: NTC $n = 1{,}056$, PINK1 $n = 1056$; non-pooled screen: NTC $n = 2{,}976$, and PINK1 $n = 2{,}976$). Accel, accelerators of parkin translocation.

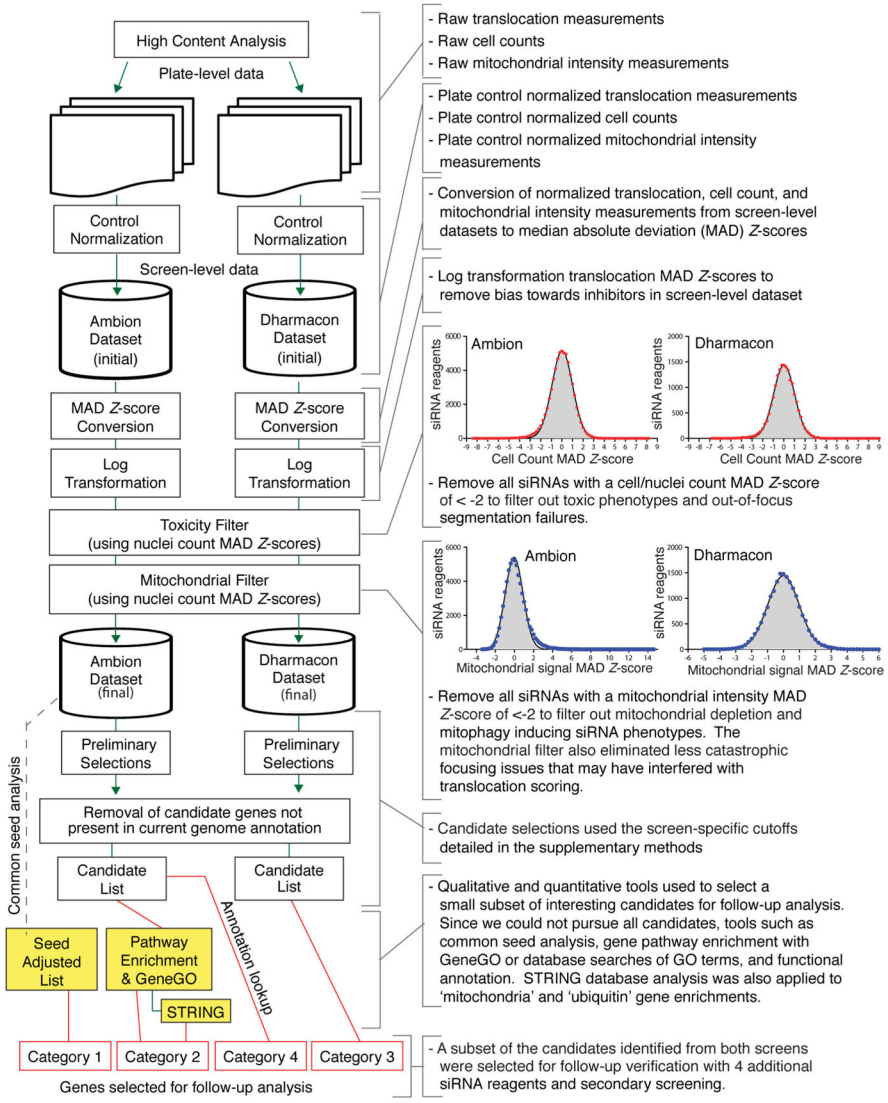

Extended Data Figure 3. Overview of data analysis workflow

Raw numerical data from high-content data generated in pooled and non-pooled screens was first normalized to the same plate controls before being stored as screen-specific data sets. Aggregate data sets underwent MAD conversion and parkin translocation data was log transformed to achieve near-normal distributions between inhibitors and accelerators. Specific siRNA-level data points were excluded if they failed to pass cell count and mitochondrial intensity filters. Data frequency distributions of cell count (red dots) fit to Gaussian curve (black line) and mitochondrial signal (blue dots) fit to a Gaussian curve (black line) from each screen are presented. Finally, gene candidates that had been withdrawn or were absent from the human genome annotation were removed from respective candidate lists. After candidate lists had been generated based on defined thresholds, a fraction of the genes were selected for follow-up analysis using a diverse set of categories to maximize selection diversity. For the non-pooled candidate lists, gene function and GO annotation queries coupled to STRING database searches (category 2) and

annotation analysis (category 4) were employed to select the most promising genes for follow-up studies. The most active gene targets from the pooled screen candidate list were also selected for follow-up analysis (category 3). Finally, a category was also developed for subset of genes having excellent seed-adjusted activity screens from common seed analysis of the non-pooled data set (category 1). See the Supplementary Methods for complete details. Green connecting arrows represent data processing or filtering operations. Red connecting lines indicate decisions made for candidate gene follow-up.

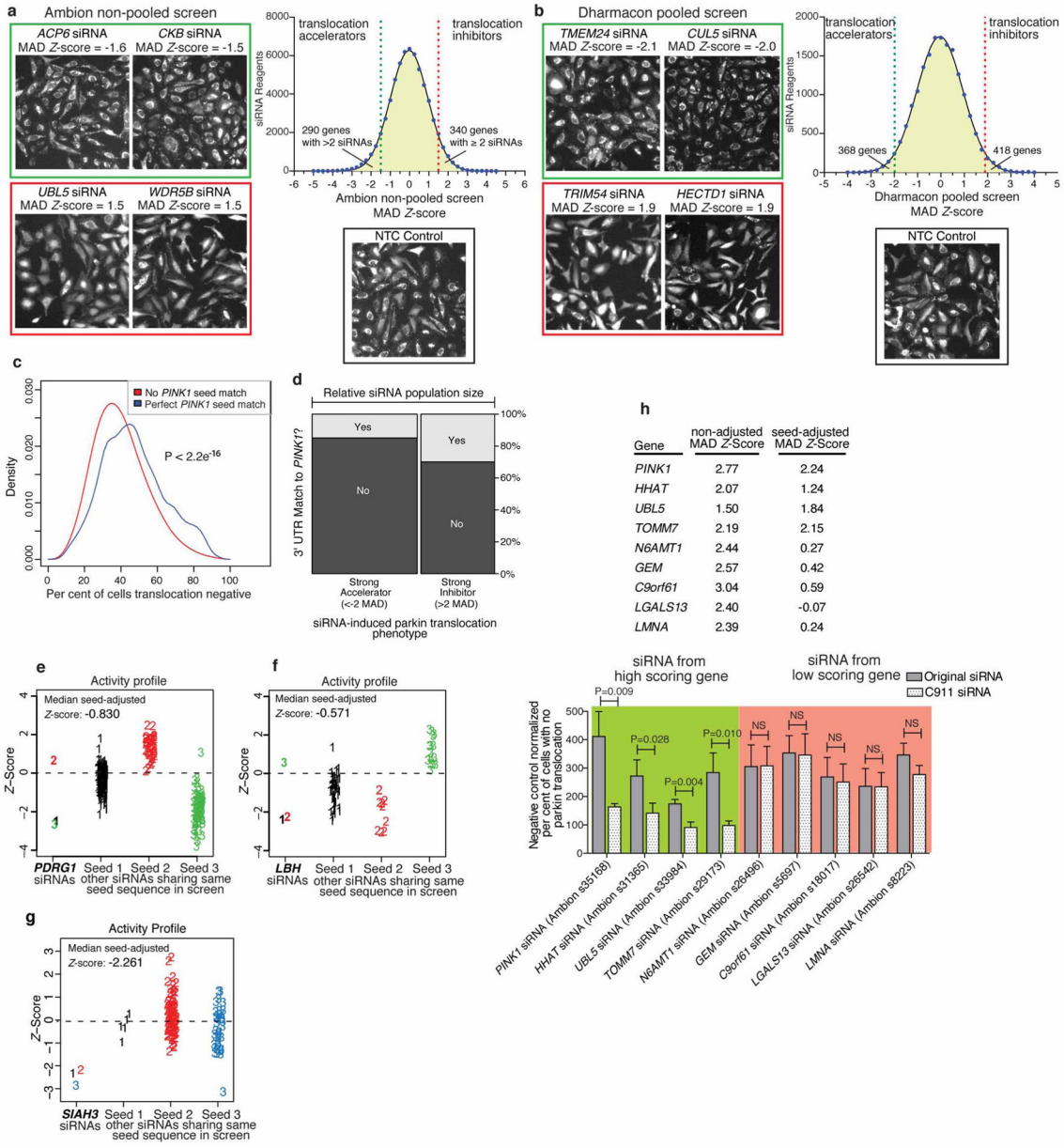

Extended Data Figure 4. Activity distributions of parkin translocation data and seed sequence bias

a, Graph of negative control (NTC siRNA) normalized, log transformed MAD *Z*-score frequency distributions of siRNA-level parkin translocation scores from the Ambion non-pooled screen. The parkin translocation cutoffs (PTC) for selecting siRNA reagents are shown with red (inhibitors) and green (accelerators) dashed lines. Representative cells from Ambion siRNA treated wells scoring near the PTC are shown (boxes are green for accelerators and red for inhibitors). Individual siRNAs meeting PTC, cytotoxicity and mitochondrial signal criteria were determined 'active'. Genes having at least two active Ambion siRNAs were selected as candidates. **b**, Same as in **a** except with the Dharmacon pooled screen data and representative images. In this data set that only had a single reagent per gene, Dharmacon siRNAs meeting PTC, cytotoxicity and mitochondrial signal criteria were selected as gene candidates. The seed sequence of a given siRNA can cause unintended modulation of gene expression through off-target, miRNA-like activity. **c**, Plot demonstrating shift in parkin translocation inhibition profile for siRNAs from the non-pooled screen whose seed sequences have a perfect match (defined in Supplementary Methods) to the 3′ UTR of *PINK1*. Statistical differences between curves assessed with a Kolmogorov–Smirnov test. **d**, Relative fractions of the highly active inhibitor (>2 MAD for parkin translocation) and accelerator (<−2 MAD for parkin translocation) siRNAs from the non-pooled screen with at least six bases of complementarity between guide strand bases 2–8 and the *PINK1* mRNA 3′ UTR (hexamer). Bar widths reflect the relative numbers of siRNAs falling into each activity population (highly inhibitory or highly accelerating to parkin translocation). Note that this analysis may only account for a small portion of siRNA off-target behaviour that directly modulates *PINK1* expression. The miRNA-like off-target effects of siRNAs in the libraries can work indirectly to affect *PINK1* expression by modulating transcription, translation and splicing (for example). **e–g**, Adjusting the activity scores of siRNAs in the context of other siRNAs that share the same seed sequence (across a non-pooled genome-wide screen) can aid in compensating for the many forms of off-target phenomena. We used this seed-activity adjustment strategy to create a composite seed-adjusted *Z*-score for each gene in our genome-wide screen of non-pooled siRNAs. As an example, *PDRG1* (**e**) and *LBH* (**f**) were both identified as highly active modulators of parkin translocation in the normalized data set. As their common seed plots reveal, the active siRNA seed sequences for these genes were biased towards acceleration of parkin translocation in the screen. This resulted in reduced seed-adjusted *Z*-scores for *PDRG1* and *LBH*, differentiating them from genes with less promiscuous siRNA seed activities such as *SIAH3* (**g**). **h**, C911 mismatch control siRNAs were assayed in 384-well plates along with their corresponding siRNA reagents (resynthesized) that had been identified as active in the primary non-pooled screen. The C911 reagents were synthesized with the same sequence and modification chemistry as the original siRNAs except that they contained the complement of bases 9, 10 and 11 of the siRNA guide strand sequence. These arrayed siRNA reagents were reverse transfected into the HeLa screening cell line as was done in the primary screen along with NTC and *PINK1* control siRNAs in the plates and translocation of parkin was assessed. Negative control normalized translocation scores (percentage of cells with no parkin translocation) were plotted for both the active siRNAs and their C911 counterparts. All of the original active siRNAs reproduced the parkin translocation inhibition displayed in the original screen (grey bars). However, the C911 analogues (white bars) of the siRNAs with minimal difference between their primary screen *Z*-score and seed-adjusted *Z*-

score (that is, the siRNAs most likely to be on-target, in the green left portion of the graph) displayed a significant reduction ($P < 0.05$ by two-tailed *t*-test) in parkin translocation inhibition. In the case of C911 analogues (white bars) of siRNAs with a low seed-corrected *Z*-score (that is, the siRNAs likely to be off-target, in the pink right portion of the graph), we observed no such reduction in activity, indicating that these siRNAs were acting through 'miRNA-like' activity (a primary driver of off-target effects). Plotted bars represent mean ± s.d. of 3 replicates. NS, not significant ($P > 0.05$).

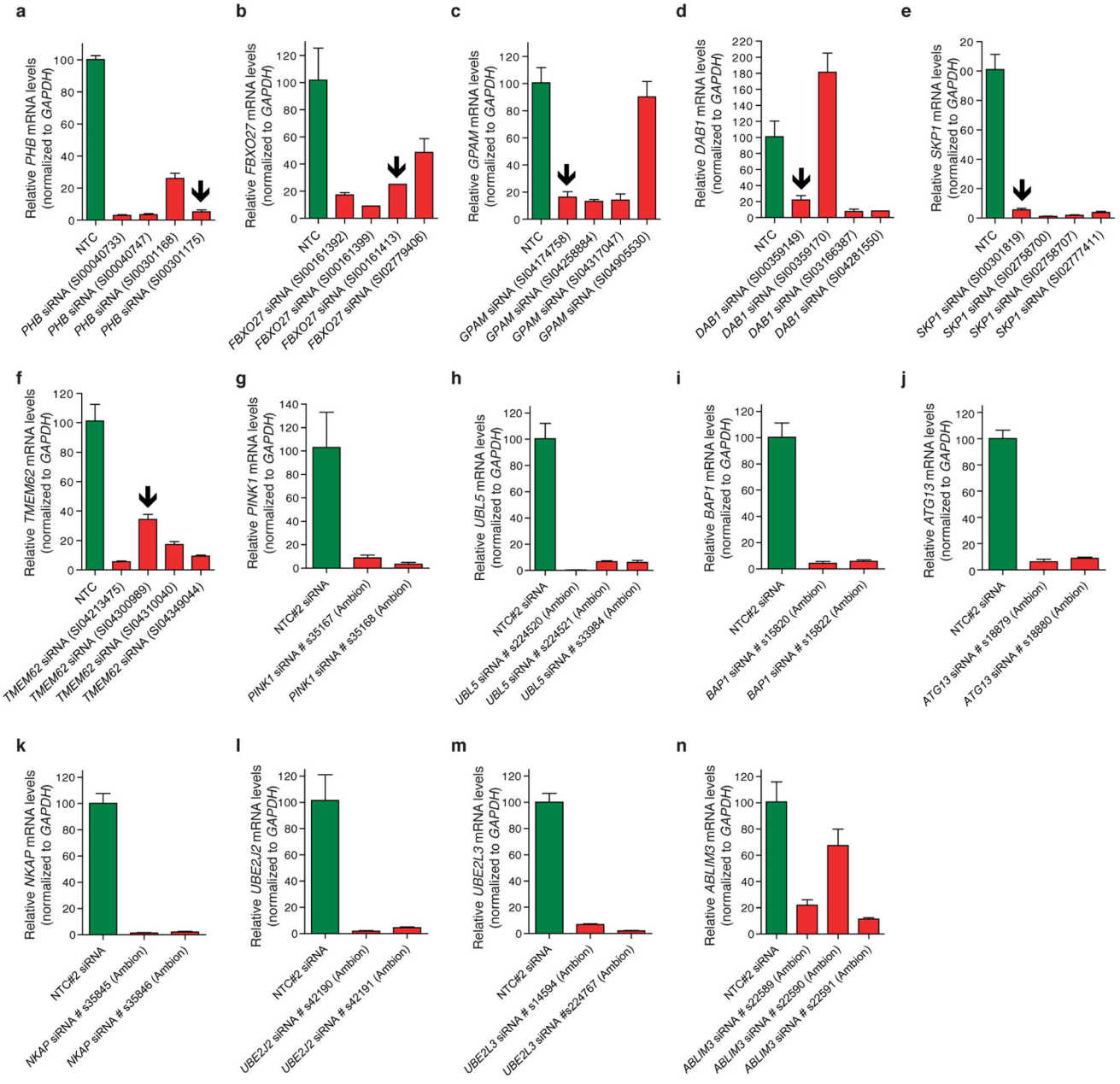

Extended Data Figure 5. Knockdown analysis of candidate reconfirmation siRNA sets with only one active siRNA reagent and of the top-ranked genes from reconfirmation experiments

a–**f**, During candidate gene reconfirmation with four Qiagen siRNAs, we observed that some candidates only displayed a single active (inhibitor of parkin translocation) siRNA in the set. To demonstrate that these are unlikely to be real regulators of parkin translocation, six of these candidates were chosen at random and investigated for Qiagen siRNA knockdown by qRT–PCR. The Qiagen siRNA sets for each candidate were arrayed in 384-plates and reverse transfected into the HeLa screening cell line as executed in the primary screen. Then mRNA was isolated from cells and converted to cDNA for qPCR after 48 h of incubation. Plots are the relative mRNA levels for *PHB* (**a**), *FBXO27* (**b**), *GPAM*(**c**), *DAB1* (**d**), *SKP1* (**e**) and *TMEM62* (**f**) targets by the specified siRNA reagents that were used in the candidate reconfirmation process. Arrows denote the only siRNA reagent that was active in inhibiting parkin translocation in the reconfirmation experiments. **g**–**n**, To demonstrate that reconfirmed genes correlated to consistent on-target knockdown by siRNA reagents in the primary screen, we resynthesized these corresponding active reagents. After executing reverse transfection into HeLa screening cell line in 384-plates (same manner as primary screen), mRNA was isolated from cells and converted to cDNA for qPCR after 48 h. Plots are the relative mRNA levels for *PINK1* (**g**), *UBL5* (**h**), *BAP1* (**i**), *ATG13* (**j**), *NKAP* (**k**), *UBE2J2* (**l**), *UBE2L3* (**m**) and *ABLIM3* (**n**) targets by the specified siRNA reagents that were originally classified as ‘active’ for parkin translocation inhibition in the primary screen (bars are mean ± s.d. of 3 technical replicates).

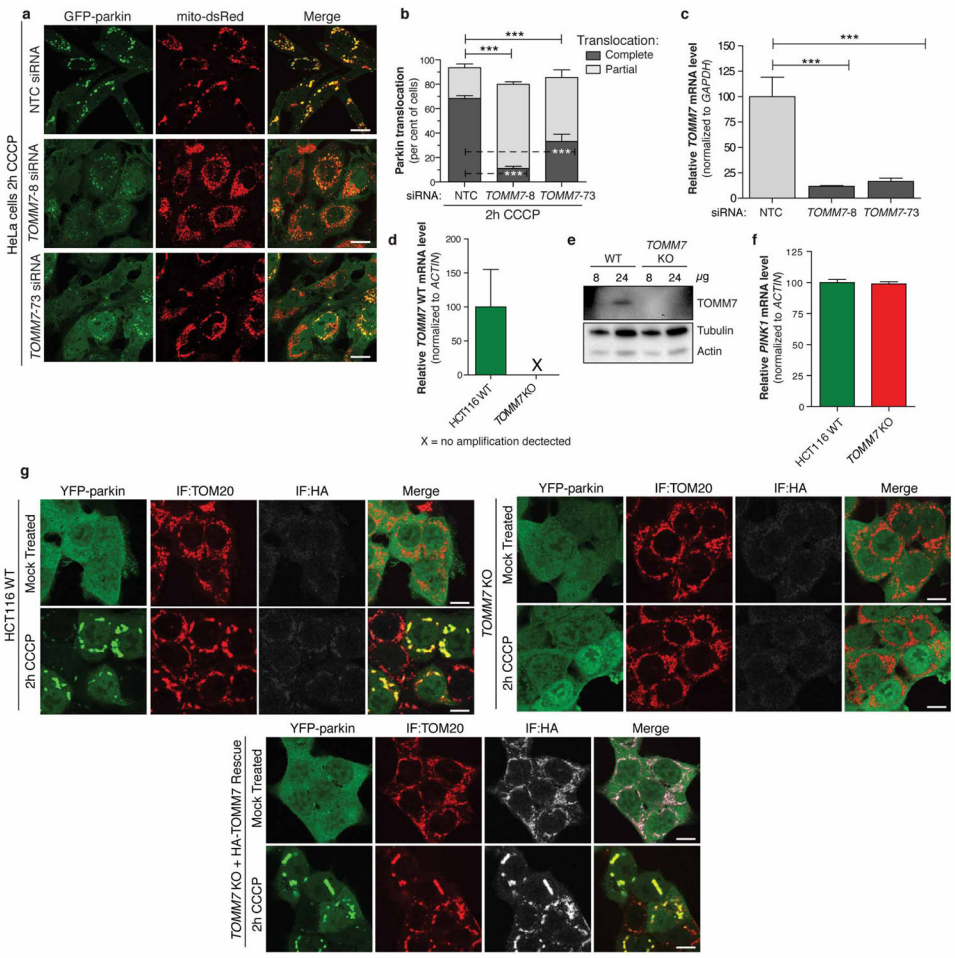

Extended Data Figure 6. TOMM7 knockdown and knockout supporting data

a, Representative images from low-throughput (in chamber slides) analysis of parkin translocation after CCCP treatment. HeLa screening cell line 48 h post-transfection with indicated siRNAs were treated with CCCP (10 µM CCCP, 2 h) and then fixed. **b**, Quantification of the translocation phenotype in **a. c**, Graph of qRT–PCR quantification of *TOMM7* mRNA levels from cells as in **a. d**, Quantification of qRT–PCR performed on mRNA transcripts isolated from wild-type (WT) or *TOMM7* knockout (KO) HCT116 cell lines using probes specific to the wild-type *TOMM7* transcript as described in the Supplementary Methods. **e**, Western blot from wild-type and *TOMM7* KO HCT116 cell lines with indicated antibodies confirming the absence of TOMM7 in the KO line. **f**, Quantification of *PINK1* mRNA by qRT–PCR performed on mRNA transcripts isolated from wild-type or *TOMM7* KO HCT116 cells. Bars in **b**, **c**, **d** and **f** represent mean ± s.d. of 3 independent experiments. mRNA levels for siRNA knockdowns are presented as a percentage of NTC samples. One-way ANOVA test were used (***$P < 0.001$). **g**, Representative images of parkin translocation after CCCP treatment (10 µM). Cells were fixed, permeabilized and stained with antibodies against TOM20 (mitochondrial marker) and HA (to verify TOMM7 expression and localization) for immunofluorescence (IF) analysis. All scale bars represent 10 µm.

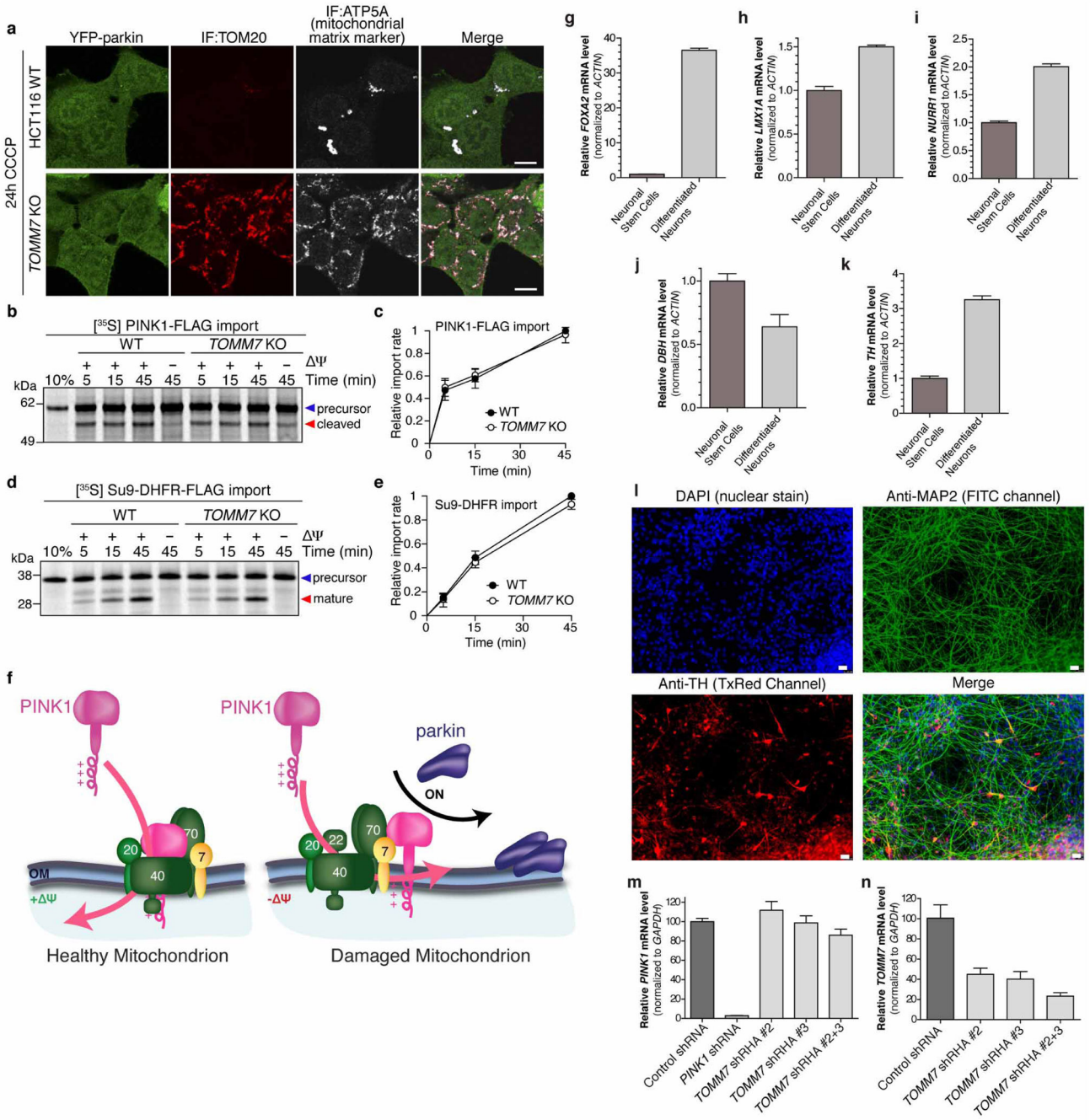

Extended Data Figure 7. TOMM7 modulates PINK1 accumulation in HCT116 cells and iPS-derived neurons

a, Representative images of mitophagy in *TOMM7* wild-type or knockout cell lines stably expressing YFP–parkin after 24 h CCCP (10 μM). Cells were fixed, permeabilized and stained with antibodies against TOM20 to detect degradation of outer mitochondrial membrane and ATP5A to detect removal of mitochondrial matrix protein. Scale bars represent 10 μm. **b**, Representative autoradiograph from PINK1 import reaction into mitochondria isolated from wild-type and *TOMM7* KO HCT116 cells. In healthy

mitochondria, imported PINK1 protein is cleaved by MPP and PARL into a mature form. However, when membrane potential is dissipated (−ΔΨ) PINK1 precursor cannot be processed. **c**, Quantification of radiolabelled PINK1 import from **b. d**, Representative autoradiograph from the canonical matrix-targeted precursor, Su9–DHFR imported into isolated mitochondria as in **b. e**, Quantification of radiolabelled Su9–DHFR import in **d. f**, Model of the function of TOMM7 in healthy and damaged mitochondria. **g–k**, Differentiation of the NSC cells into iPS-derived neurons was validated with qRT–PCR of mRNA isolated from cells before and following the process. **g**, Gene expression of *FOXA2* (critical signal promoting the initial development of dopaminergic neurons) and **h**, *LMX1A* (part of a transcriptional loop that acts to promote the development of mature DA neurons). **i**, Gene expression of *NURR1* (also known as *NR4A1*) a commonly used marker for the early stages of dopaminergic neuron differentiation. **j**, Gene expression of dopamine beta-hydroxylase (*DBH*), an enzyme that catalyses the conversion of dopamine to norepinephrine in sympathetic neurons of the adrenal medulla. *DBH* was used as a negative control in these experiments as it should not increase in NSCs differentiated into a dopaminergic fate. **k**, Gene expression of tyrosine hydroxylase (TH) as a marker of dopaminergic neuron differentiation. **l**, Representative field from immunofluorescence imaging of NSCs that had completed the neuronal differentiation process and then been fixed and stained. Microtubule-associated protein 2 (MAP2) is general neuronal marker. White scale bars represent 100 μm. **m**, *PINK1* mRNA levels from iPS-derived neurons that had been infected with lentiviral shRNA constructs. **n**, *TOMM7* mRNA levels from the same set of lentivirus-treated samples was measured to verify the knockdown. All qRT–PCR experiments are plotted as mean ± s.d. of $n = 3$ technical replicates.

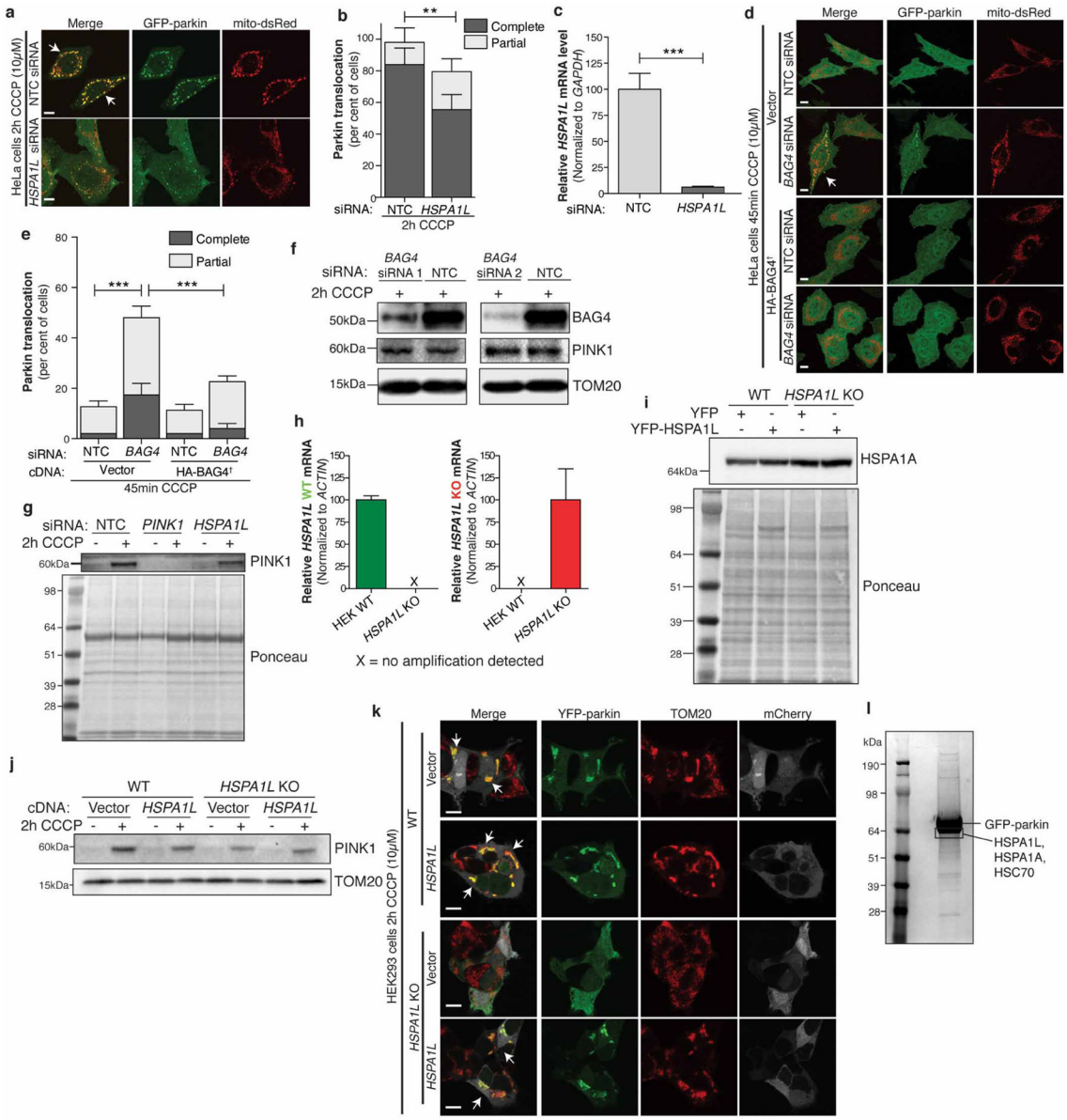

Extended Data Figure 8. HSPA1L and BAG4 supporting data

a, Representative screening HeLa cells confirming *HSPA1L* siRNA knockdown phenotype after 2 h CCCP treatment (10 μM) using NTC siRNA or *HSPA1L* siRNA. Images display GFP–parkin (green) and mitochondrial dsRed (red). **b**, Quantification of the parkin translocation defect under the conditions in **a. c**, qRT–PCR of *HSPA1L* mRNA transcripts isolated from cells as in **a. d**, Representative images of parkin translocation in GPRM2 HeLa cells with gene knockdown of *BAG4* and rescue (HA–*BAG4*† cDNA) after 45 min CCCP treatment (10 μM). The *BAG4*† is siRNA resistant cDNA. **e**, Quantification of phenotype observed in **d. f**, Western blots of BAG4 and PINK1 total protein levels from GPRM cells transfected with either NTC or *BAG4* siRNAs and treated for 2 h with CCCP. There is a large decrease in the level ofBAG4 protein in the knockdown compared to controls, but PINK1 levels are unchanged. **g**. Western blot of PINK1 from cells transfected with NTC,

PINK1 or *HSPA1L* siRNA and Ponceau total protein stain for loading control. Cells were treated with CCCP for 2 h to induce PINK1 stabilization and *HSPA1L* knockdown does not affect PINK1 levels. **h**, qRT–PCR of mRNA transcripts isolated from wild-type or *HSPA1L* knockout HEK cell lines using probes specific to the wild-type (WT) or mutated transcript (KO) as described in the Supplementary Methods section. **i**, Western blotting with the specific HSPA1A antibody revealed that HSPA1Aprotein levels are unaffected in the *HSPA1L*KOcell line, and Ponceau total protein stain for loading control. **j**, PINK1 western blots from wild-type and *HSPA1L* knockout cells lines that have been transfected with either vector control or mCherry–*HSPA1L*. PINK1 levels are not detectable in the absence of CCCP and are comparable in both the wild-type and knockout after CCCP treatment, regardless of *HSPA1L* rescue. **k**, Images relating to Fig. 4a examining YFP–parkin translocation in wild-type and *HSPA1L* knockout HEK293 cells at 2 h of CCCP treatment. Cells were either transfected with an empty mCherry vector or mCherry–*HSPA1L* to rescue the knockout phenotype. **l**, GFP–parkin was immunoprecipitated from the HeLa screening cell line and the indicated bands were excised for mass spectrometry analysis. Observed HSP70 proteins are indicated (see Supplementary Table 9 for peptide data). Bars in **b**, **c**, **e** and **h** are mean ± s.d. of 3 independent replicates with significance tested by a one-way ANOVA. White arrows indicate cells with complete parkin translocation.

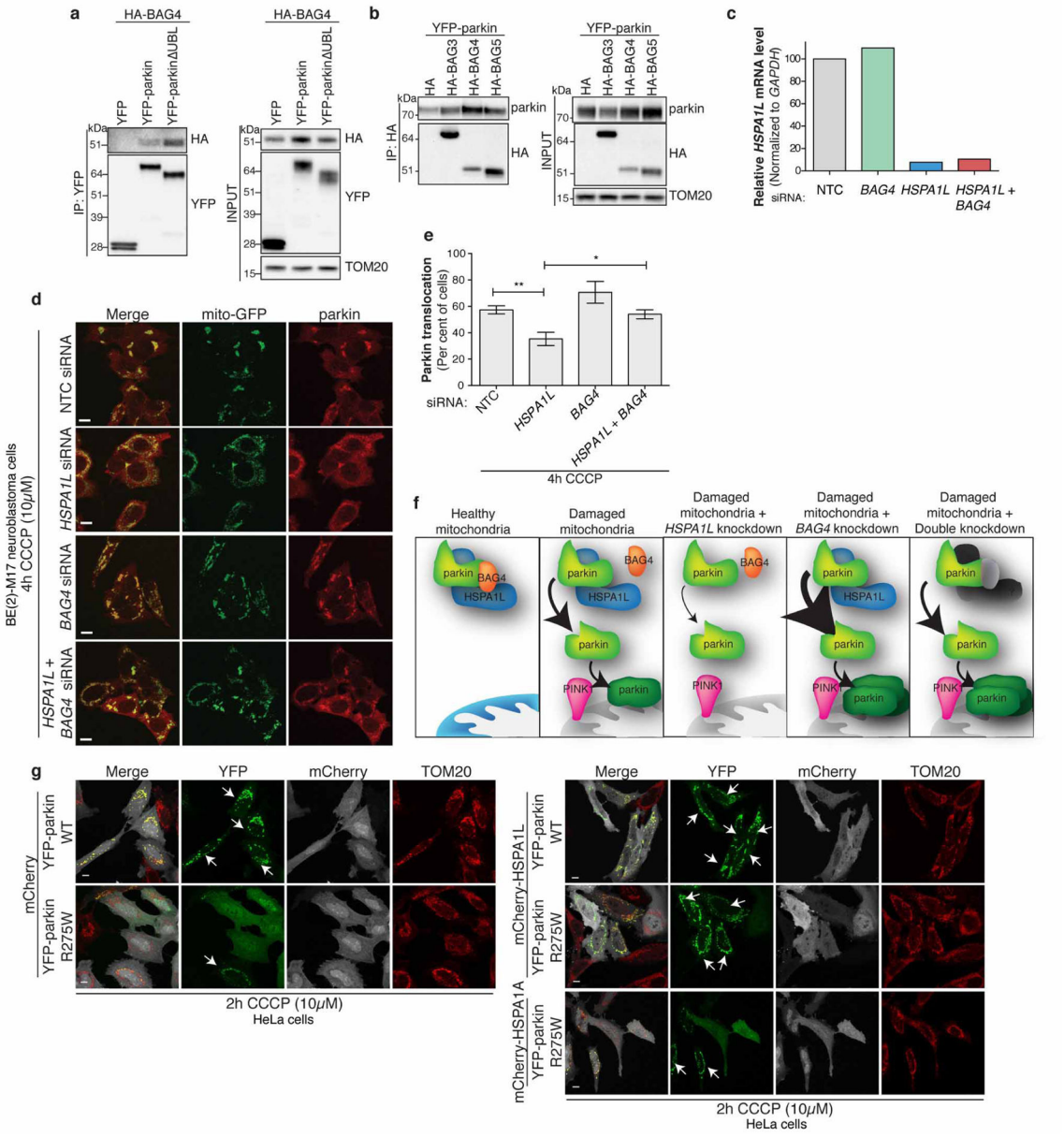

Extended Data Figure 9. Parkin and BAG4 binding and HSPA1L and BAG4 knockdown

a, Representative western blot of immunoprecipitation of YFP–parkin or YFP–parkin ΔUBL in HeLa cells. HA–BAG4 is bound to YFP–parkin and binds more strongly to YFP–parkin ΔUBL. **b**, Representative images of HA immunoprecipitations using either the empty vector or HA–BAG3, HA–BAG4 or HA–BAG5 in HeLa cells. YFP–parkin shows some binding to all three BAG family members, but is bound at the highest level to HA–BAG4. **c**, Quantitation of qRT–PCR of *HSPA1L* mRNA transcripts from cells transfected with NTC, *BAG4*, *HSPA1L* or *BAG4* plus *HSPA1L* siRNA in HeLa cells. *HSPA1L* is knocked down to comparable levels in both the signal (*HSPA1L* alone) and double (*BAG4* plus *HSPA1L*) siRNA experiments. **d**, Representative images of parkin translocation in the BE(2)-M17 neuroblastoma cell line stably expressing mitochondrial GFP and native (untagged) parkin

transfected with the indicated siRNAs, following 4 h CCCP treatment. Parkin localization was detected by immunofluorescence (red). Scale bars represent 10 μm. **e**, Quantification of **d** from three independent experiments (>150 cells were counted per condition) and displayed as mean ± s.d. and use of one-way ANOVA tests (*$P < 0.05$, ** $P < 0.01$). **f**, Model of the potential mechanism of BAG4/HSPA1L regulation of parkin. **g**, Single channel images of wild-type YFP–parkin and YFP–parkin(R275W) translocation with or without the coexpression of mCherry–*HSPA1L* or *HSPA1A* corresponding to Fig. 4f in the main text. White arrows indicate cells with complete parkin translocation. All immunoprecipitation experiments were performed in transiently transfected HeLa cells and are shown as representative images of three independent experiments.

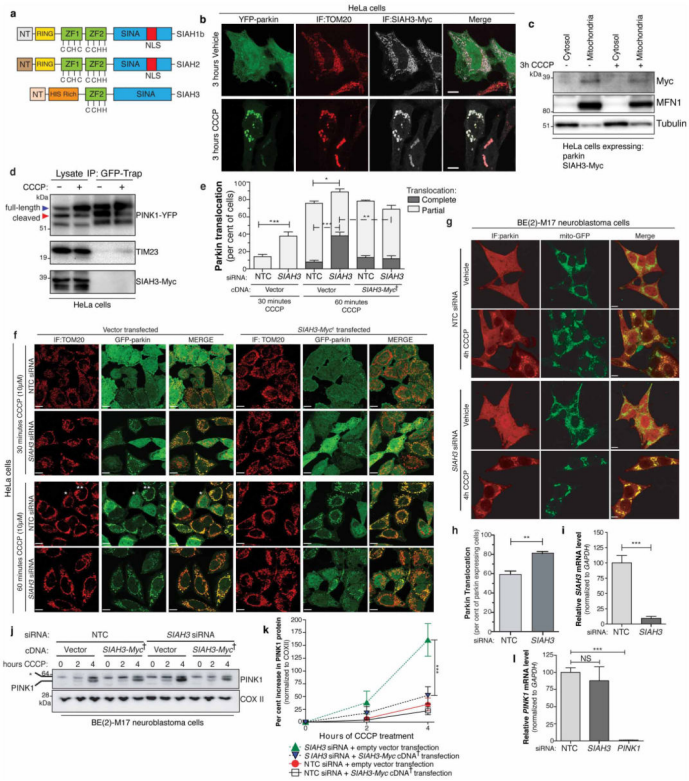

Extended Data Figure 10. SIAH3 is a negative regulator of parkin translocation

a, Domain structure within the human SIAH family. Domains include non-conserved N-terminal regions (NT), two zinc-finger motifs (ZF1 and ZF2), a nuclear localization sequence (NLS), and the Seven in absentia (SINA) protein superfamily C-terminal substrate binding domain. SIAH3 contains a unique histidine rich (HIS Rich) region. Conserved histidines and cysteines found in the zinc-finger regions are denoted with H and C, respectively. **b**, Representative images from *SIAH3*-Myc expression in HeLa cells with and without 3 h CCCP treatment. IF, immunofluorescence, from antibodies towards specified targets (TOM20 or Myc). **c**, By western blot, SIAH3–Myc is present primarily in the mitochondrial fraction of cell extracts. **d**, Immunoprecipitation of PINK1–YFP from HeLa cells transiently transfected with both *PINK1*–YFP and *SIAH3*–Myc. **e**, Quantification of parkin translocation after 30 or 60 min of 10 μM CCCP treatment under the conditions in **f**

from 3 independent experiments (>150 cells were counted per condition). Bars represent mean ± s.d. One-way ANOVA was used to determine the significance of comparisons; *$P <$ 0.05 **$P < 0.01$, ***$P < 0.001$. Bracketing lines between bars indicate comparison of partial (solid) or complete (dashed) parkin translocation. **f**, Representative images (GFP–parkin in green and Tom20 immunofluorescence plus mitochondrial dsRed in red) of screening HeLa cells from independent confirmation of gene knockdown (NTC siRNA versus *SIAH3* siRNA) and rescue (vector-only versus *SIAH3*† cDNA overexpression) phenotypes after 30 or 60 min CCCP treatment (10 μM). The *SIAH3*† is siRNA resistant cDNA. **g**, BE(2)-M17 cell line stably expressing mitochondrial GFP and native (untagged) parkin transfected with NTC or *SIAH3* siRNA. Since BE(2)-M17 cells were expressing a low amount of parkin and they displayed a slower translocation phenotype, parkin translocation was assessed after 4 h of CCCP. **h**, Quantification of **g** from three independent experiments (>150 cells were counted per condition). **i**, qRT–PCR quantification of *SIAH3* mRNA knockdown 48 h after indicated siRNAs were transfected into BE(2)-M17 cells. **j**, Representative western blot of BE(2)- M17 cell lysates from cells transfected with the indicated siRNA or cDNA combination for 48 h and then treated with 10 μM CCCP for 0, 2 or 4 h. In western blots of BE(2)-M17 cell lysates, an indicated non-specific band is present above the indicated PINK1 band (*) when probed with PINK1 antibody. **k**, Quantification of **j** represented as COXII normalized signal from PINK1 bands as a percentage relative to the 0 h CCCP PINK1 reference band. **l**, qRT–PCR quantification of relative *PINK1* mRNA levels after 48 h following indicated siRNA transfection into HeLa cells. NS, not significant. Quantifications are displayed as mean ± s.d. of 3 independent experiments, One-way ANOVA were used to determine the significance of comparisons.

Acknowledgments

We thank P. Tuzmen for qRT–PCR assistance; C. Klumpp for automation; D. Maric for FACS sorting; C. Smith for microscopy assistance; H. Jaffe for mass spectrometry analyses; R. Fields (NINDS) for lentivirus assistance; N. Malik for iPS-derived neurons; the NINDS DNA Sequencing Facility; K. Mihara for the TOMM7 antibody and A. Koretsky and N. Caplen for support. Research was supported by the Japan Society for Promotion of Science Postdoctoral Fellowship for Research Abroad (K.Y.), the NIGMS Research Associate Program, the Intramural Research Program of the NIH, NINDS and the Trans-NIH RNAi initiative.

References

1. Schapira AH, Tolosa E. Molecular and clinical prodrome of Parkinson disease: implications for treatment. Nature Rev Neurol. 2010; 6:309–317. [PubMed: 20479780]
2. Valente EM, et al. Hereditary early-onset Parkinson's disease caused by mutations in *PINK1.* Science. 2004; 304:1158–1160. [PubMed: 15087508]
3. Kitada T, et al. Mutations in the *parkin* gene cause autosomal recessive juvenile parkinsonism. Nature. 1998; 392:605–608. [PubMed: 9560156]
4. Vincow ES, et al. The PINK1–Parkin pathway promotes both mitophagy and selective respiratory chain turnover *in vivo*. Proc Natl Acad Sci USA. 2013; 110:6400–6405. [PubMed: 23509287]
5. Narendra D, Tanaka A, Suen DF, Youle RJ. Parkin is recruited selectively to impaired mitochondria and promotes their autophagy. J Cell Biol. 2008; 183:795–803. [PubMed: 19029340]
6. Narendra DP, et al. PINK1 is selectively stabilized on impaired mitochondria to activate Parkin. PLoS Biol. 2010; 8:e1000298. [PubMed: 20126261]
7. Vives-Bauza C, et al. PINK1-dependent recruitment of Parkin to mitochondria in mitophagy. Proc Natl Acad Sci USA. 2010; 107:378–383. [PubMed: 19966284]

8. Geisler S, et al. PINK1/Parkin-mediated mitophagy is dependent on VDAC1 and p62/SQSTM1. Nature Cell Biol. 2010; 12:119–131. [PubMed: 20098416]
9. Sarraf SA, et al. Landscape of the PARKIN-dependent ubiquitylome in response to mitochondrial depolarization. Nature. 2013; 496:372–376. [PubMed: 23503661]
10. Chan NC, et al. Broad activation of the ubiquitin-proteasome system by Parkin is critical for mitophagy. Hum Mol Genet. 2011; 20:1726–1737. [PubMed: 21296869]
11. Gautier CA, Kitada T, Shen J. Loss of PINK1 causes mitochondrial functional defects and increased sensitivity to oxidative stress. Proc Natl Acad Sci USA. 2008; 105:11364–11369. [PubMed: 18687901]
12. Pimenta de Castro I, et al. Genetic analysis of mitochondrial protein misfolding in *Drosophila melanogaster*. Cell Death Differ. 2012; 19:1308–1316. [PubMed: 22301916]
13. Suen DF, Narendra DP, Tanaka A, Manfredi G, Youle RJ. Parkin overexpression selects against a deleterious mtDNA mutation in heteroplasmic cybrid cells. Proc Natl Acad Sci USA. 2010; 107:11835–11840. [PubMed: 20547844]
14. Burman JL, Yu S, Poole AC, Decal RB, Pallanck L. Analysis of neural subtypes reveals selective mitochondrial dysfunction in dopaminergic neurons from *parkin* mutants. Proc Natl Acad Sci USA. 2012; 109:10438–10443. [PubMed: 22691499]
15. Sigoillot FD, King RW. Vigilance and validation: keys to success in RNAi screening. ACS Chem Biol. 2011; 6:47–60. [PubMed: 21142076]
16. Bushman FD, et al. Host cell factors in HIV replication: meta-analysis of genome-wide studies. PLoS Pathog. 2009; 5:e1000437. [PubMed: 19478882]
17. Simpson JC, et al. Genome-wide RNAi screening identifies human proteins with a regulatory function in the early secretory pathway. Nature Cell Biol. 2012; 14:764–774. [PubMed: 22660414]
18. Schultz N, et al. Off-target effects dominate a large-scale RNAi screen for modulators of the TGF-β pathway and reveal microRNA regulation of TGFBR2. Silence. 2011; 2:3. [PubMed: 21401928]
19. Sudbery I, Enright AJ, Fraser AG, Dunham I. Systematic analysis of off-target effects in an RNAi screen reveals microRNAs affecting sensitivity to TRAIL-induced apoptosis. BMC Genomics. 2010; 11:175. [PubMed: 20230625]
20. Jackson AL, et al. Widespread siRNA "off-target" transcript silencing mediated by seed region sequence complementarity. RNA. 2006; 12:1179–1187. [PubMed: 16682560]
21. Birmingham A, et al. 3′ UTR seed matches, but not overall identity, are associated with RNAi off-targets. Nature Methods. 2006; 3:199–204. [PubMed: 16489337]
22. Buehler E, et al. siRNA off-target effects in genome-wide screens identify signaling pathway members. Sci Reports. 2012; 2:428.
23. Marine S, Bahl A, Ferrer M, Buehler E. Common seed analysis to identify off-target effects in siRNA screens. J Biomol Screen. 2012; 17:370–378. [PubMed: 22086724]
24. Buehler E, Chen YC, Martin S. C911: A bench-level control for sequence specific siRNA off-target effects. PLoS ONE. 2012; 7:e51942. [PubMed: 23251657]
25. Kato H, Mihara K. Identification of Tom5 and Tom6 in the preprotein translocase complex of human mitochondrial outer membrane. Biochem Biophys Res Commun. 2008; 369:958–963. [PubMed: 18331822]
26. Jin SM, et al. Mitochondrial membrane potential regulates PINK1 import and proteolytic destabilization by PARL. J Cell Biol. 2010; 191:933–942. [PubMed: 21115803]
27. Lazarou M, Jin SM, Kane LA, Youle RJ. Role of PINK1 binding to the TOM complex and alternate intracellular membranes in recruitment and activation of the E3 ligase Parkin. Dev Cell. 2012; 22:320–333. [PubMed: 22280891]
28. Moore DJ, West AB, Dikeman DA, Dawson VL, Dawson TM. Parkin mediates the degradation-independent ubiquitination of Hsp70. J Neurochem. 2008; 105:1806–1819. [PubMed: 18248624]
29. Kalia SK, et al. BAG5 inhibits parkin and enhances dopaminergic neuron degeneration. Neuron. 2004; 44:931–945. [PubMed: 15603737]
30. Hageman J, Kampinga HH. Computational analysis of the human HSPH/HSPA/DNAJ family and cloning of a human HSPH/HSPA/DNAJ expression library. Cell Stress Chaperones. 2009; 14:1–21. [PubMed: 18686016]

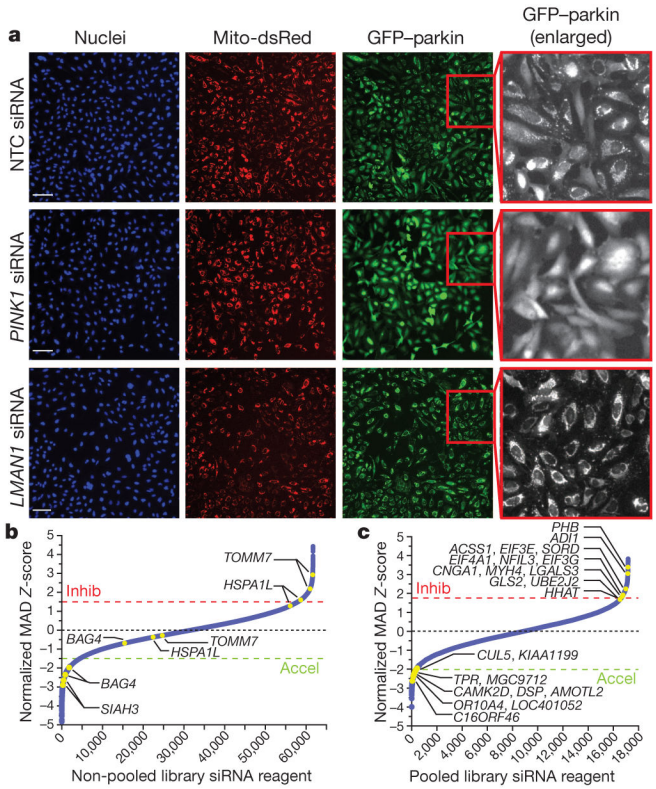

Figure 1. A high-content screening assay for regulators of parkin translocation in HeLa cells following mitochondrial damage

a, Representative images of parkin translocation assay. NTC (non-targeting control), *PINK1* (inhibited translocation) and *LMAN1* (accelerated translocation) siRNA transfected cells from genome-wide screens. Red-boxed panels are magnified views of GFP–parkin. Scale bars, 100 μm. **b**, Negative control normalized, log transformed MAD *Z*-scores of all non-pooled reagents; data ordered from most negative to positive. Dashed red (inhibitors, Inhib) or green lines (accelerators, Accel) are screen-specific cutoffs (see Supplementary Methods) for active siRNA reagents. Yellow dots represent genes explored in this manuscript. **c**, Same as **b** but for the pooled RNAi screen; yellow dots represent overlap of candidate gene selections between pooled and non-pooled RNAi screens.

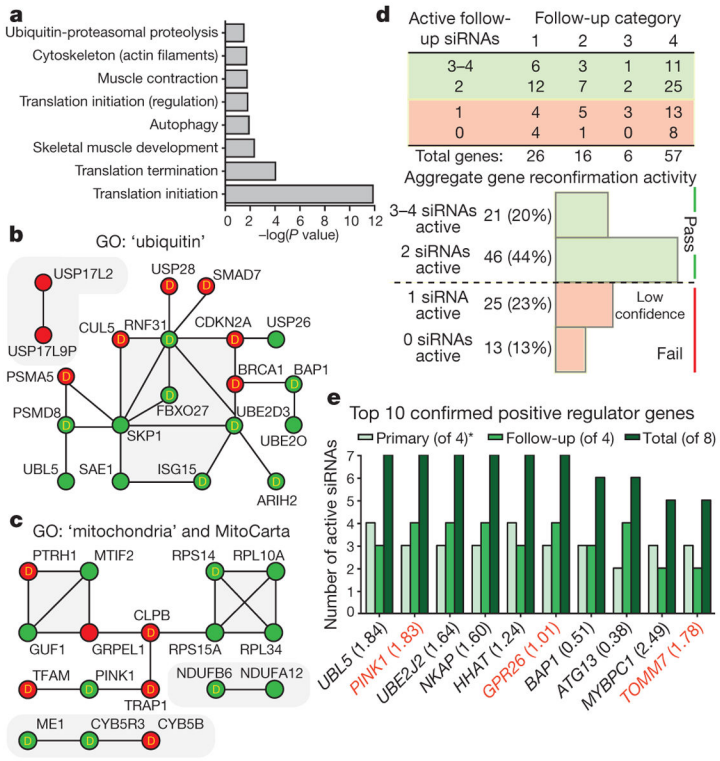

Figure 2. Analysis of active siRNAs revealed linked gene clusters and sources of off-target effects

a, GeneGo cellular processes of candidate genes with significant enrichments (*P*-value cutoff of 0.05) (Supplementary Table 1). **b**, Candidate genes with ontology (GO) that included 'ubiquitin' and interactions by STRING association. Gene nodes are coloured green (positive regulator), red (negative regulator) and contain 'D' if they are members of the 'druggable' genome. **c**, Same as **b** but for the GO term 'mitochondria' or matches to the human MitoCarta database. **d**, Analysis of group specific (top panel) and aggregate (bottom panel) reconfirmation results (percentages are out of 105 tested). **e**, Top 10 positive regulator genes that passed reconfirmation (≥2 active siRNAs) in order of total active siRNAs and ties settled by seed-adjusted *Z*-score. Numbers in brackets indicate seed-adjusted *Z*-scores and red lettering indicates genes whose knockdown blocked PINK1 accumulation (see Supplementary Table 7). Asterisk indicates inclusion of siRNAs passing 'active' thresholds only in raw and non-transformed data sets because they exhibited excellent phenotypes upon inspection. Analyses in **a–c** were performed on original non-pooled candidate list (Supplementary Table 1) and **d**, **e** were performed on the candidates chosen for reconfirmation assays (Supplementary Table 6).

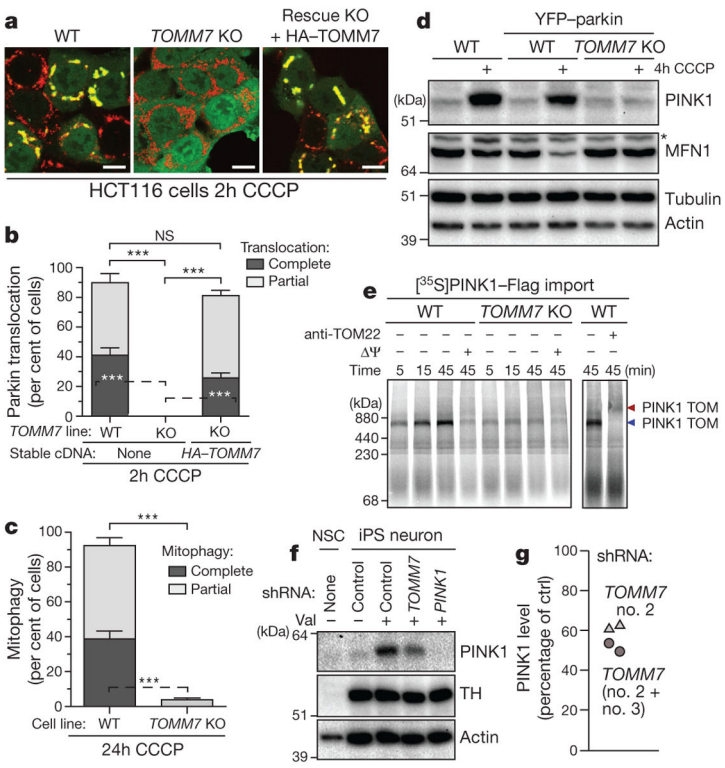

Figure 3. Characterization of *TOMM7*, a positive regulator of parkin translocation

a, Representative images of HCT116 cells stably expressing YFP–parkin (green) after 2 h of CCCP treatment: wild-type (WT), *TOMM7* knockout (KO), or *TOMM7* KO with stable expression of HA–*TOMM7*. Mitochondria are indicated by TOM20 immunofluorescence (red). **b**, Quantification of parkin translocation in **a. c**, Quantification of mitophagy observed using cells in **a** (24 h of CCCP) as measured by the loss of TOM20 and ATP5A signal (See Extended Data Fig. 7a). **d**, Western blot of whole-cell lysates from cells in **a** or wild-type HCT116 (lacking parkin) treated with CCCP for 0 or 4 h. An asterisk indicates a non-specific band. **e**, Blue native polyacrylamide gel electrophoresis (PAGE) import reactions (left) and super-shift (right) assay illustrate PINK1 association with the TOM complex. Blue arrow indicates PINK1 association with the TOM complex, red arrow indicates complex shifted by TOM22 antibody. **f**, Western blot of PINK1 and tyrosine hydroxylase (TH) levels in neuronal stem cells (NSC) and iPS-derived neurons. **g**, Quantification of PINK1 levels in **f**, expressed as the percentage of control levels ($n = 4$, $P < 0.001$ compared to control shRNA). Cells were infected with *TOMM7* shRNA no. 2 (triangles) or both no. 2 and no. 3 (circles). Quantification in **b** and **c** represent three independent experiments (>150 cells were counted per condition), are displayed as mean ± s.d. and using one-way ANOVA tests (***$P < 0.001$). CCCP, 10 μM. Scale bar; 10 μm. For single channel images of **a** see Extended Data Fig. 6g.

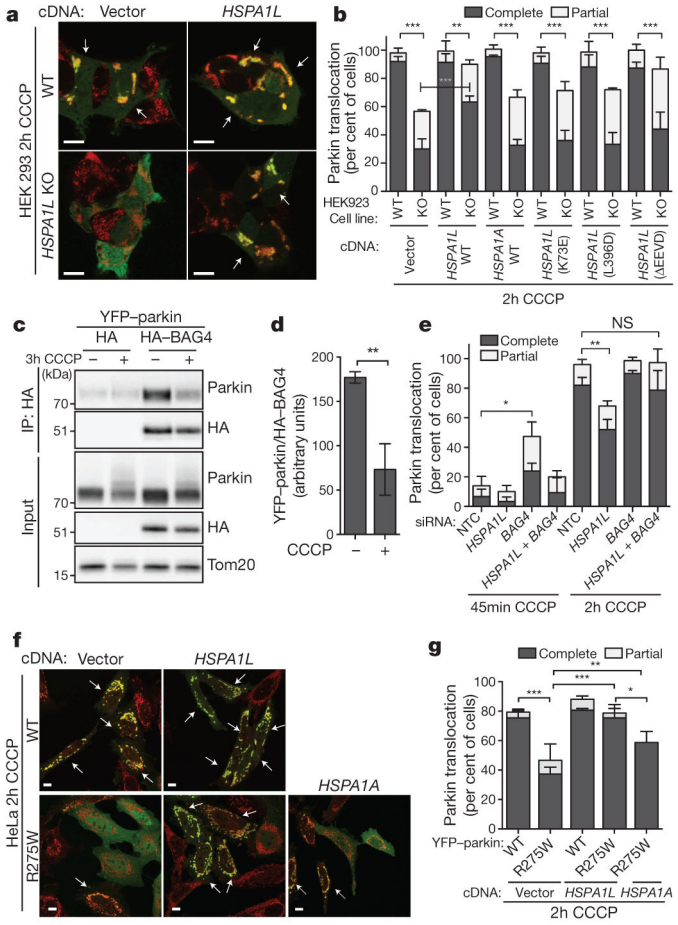

Figure 4. HSPA1L and BAG4 differentially modulate translocation of parkin to damaged mitochondria

a, Representative images of wild-type (WT) and HSPA1L knockout (KO) HEK293 cells after 2 h CCCP with either mCherry vector or mCherry–HSPA1L overexpression showing rescue (YFP–parkin (green), Tom20 (red)). **b**, Quantification of parkin translocation from **a** and other rescue attempts. **c**, YFP–parkin is present in immunopreciptates of HA–BAG4. **d**, Quantification of the intensity of bands in **c** ($n = 3$). **e**, siRNA knockdown of both *BAG4* and *HSPA1L* abrogates the phenotype of either individual gene knockdown. **f**, Translocation of parkin patient mutation R275W. **g**, Quantification of **f**. Quantification in **b**, **e** and **g** represent three independent experiments (>150 cells were counted per condition), are mean ± s.d.; one-way ANOVA tests (*$P < 0.05$, **$P < 0.01$ and ***$P < 0.001$). Statistical comparisons are displayed for only complete translocation phenotype. CCCP, 10 μM. White arrows indicate cells with complete parkin translocation. Scale bars, 10 μm. For single channel images of **a** and **f** see Extended Data Figs 8k and 9g.